The Astrophysical Journal, 623:242–251, 2005 April 10

A CANDIDATE ANALOG FOR CARBONACEOUS INTERSTELLAR DUST: FORMATION BY REACTIVE PLASMA POLYMERIZATION

E. Kovačević,[1] I. Stefanović,[1,2] J. Berndt,[1] Y. J. Pendleton,[3] and J. Winter[1]

Received 2004 June 1; accepted 2004 December 19

ABSTRACT

Carbonaceous compounds are a significant component of interstellar dust, and the composition and structure of such materials is therefore of key importance. We present 1.5–15 μm spectra of a plasma-polymerized carbonaceous material produced in radio-frequency discharge under low pressure, using C_2H_2 as a precursor component. The infrared spectra of the resulting spheroidal carbonaceous nanoparticles reveal a strong aliphatic band (3.4 μm feature), weak OH and carbonyl bands, and traces of aromatic compounds, all characteristics identified with dust in the diffuse interstellar medium of our Galaxy. The plasma polymerization process described here provides a convenient way to make carbonaceous interstellar dust analogs under controlled conditions and to compare their characteristics with astronomical observations. Here we focus on a comparison with the IR spectra of interstellar dust. The IR spectrum of carbonaceous dust in the diffuse interstellar medium is characterized by a strong 3.4 μm C—H stretching band and weak 6.8 and 7.2 μm C—H bending bands, with little evidence for the presence of oxygen in the form of carbonyl (C=O) or hydroxide (OH) groups. The plasma polymerization products produced under oxygen-poor conditions compare well with the peak position and profiles of the observed IR spectrum of diffuse dust. In addition, we find that addition of nitrogen to the plasma results in bands at 6.15 μm (C=N band) and at 3 μm (NH band). We note that, with the addition of nitrogen, the 3.4 μm hydrocarbon band diminishes greatly in strength as the NH band grows. This may have implications for the puzzling absence of the 3.4 μm hydrocarbon bands in the IR spectra of dust in dense molecular clouds, given that the presence of nitrogen-related bands has been established in dense-cloud dust.

Subject headings: astrochemistry — dust, extinction — infrared: ISM — ISM: lines and bands — line: identification — methods: laboratory

1. INTRODUCTION

Dust particles are ubiquitous in space, occurring in diffuse and in dense interstellar mediums (Sandford et al. 1991; Pendleton et al. 1994; Whittet et al. 1997), circumstellar shells (Gauger et al. 1990), the dark interiors of molecular clouds (Neckel & Staude 1987), stellar envelopes (Jura 1990), nova ejecta (Gehrz et al. 1998), the outflow of red giant stars and proto–planetary nebulae (Cassinelli 1979; Woolf & Ney 1969; Chiar et al. 1998), and the interstellar medium of other galaxies (Spoon et al. 2003; Mason et al. 2004). Even though interstellar gas dominates the mass balance by a factor of 100, dust plays an important role in the interstellar medium (ISM). In particular, interstellar dust regulates star formation, catalyzes molecule production, and reprocesses UV and optical radiation. A useful tracer of the carbonaceous component of dust is the C—H stretch of aliphatic hydrocarbons observed in absorption at 3.4 μm throughout the Galactic diffuse ISM (DISM) (see Pendleton 2004 for a review). The identification of solid hydrogenated carbonaceous material in the DISM has been confirmed by infrared observations and has been extensively studied in the laboratory (see Pendleton & Allamandola 2002 for a review). Strong observational evidence is based upon the ubiquitous absorption feature at 3.4 μm, now detected along nearly two dozen sight lines through diffuse dust in our Galaxy (Butchart et al. 1986; Adamson et al. 1990; Sandford et al. 1991; Pendleton et al. 1994; Pendleton 1997b; Whittet et al. 1997; Rawlings et al. 2003), as well as in the rest-frame spectra of several nearby galaxies (Bridger et al. 1994; Mizutani et al. 1994; Wright et al. 1996; Imanishi et al. 1997; Imanishi 2000a, 2000b; Imanishi & Dudley 2000; Imanishi et al. 2001; Imanishi 2002; Imanishi & Maloney 2003; Marco & Brooks 2003; Risaliti et al. 2003). The UV extinction bump seen at 2175 Å is also clear evidence of a carbonaceous component in the DISM, and many proposed materials have been invoked to explain this feature. It is now generally accepted that nanometer-sized carbon grains play a fundamental role as the carrier of the UV bump (Mennella et al. 2004). Some have suggested the UV bump and the 3.4 μm absorption band arise from the same material. In the laboratory, the C—H stretching bands near 3.4 μm are always accompanied by C—H bending-mode bands in the 6–8 μm region, the exact positions being determined by the composition of the aliphatic hydrocarbon chains. Observationally, the 3.4 μm band is accompanied by two weak bending-mode bands at longer wavelengths, which occur at 6.8 and 7.2 μm (Chiar et al. 2000) in dusty sight lines toward the Galactic center.

Because of the extreme luminosity of the Galactic center and the large column density of interstellar dust along that line of sight, absorption features that reveal the composition of the intervening dust are readily observed. The 3.4 μm band was first detected toward the Galactic center (Soifer et al. 1976) and has been studied in detail by many (e.g., Sandford et al. 1991; Allamandola et al. 1992; Pendleton et al. 1994; Adamson et al. 1999). As reported by Sandford et al. (1991), and supported by laboratory work, the spectral profile of the 3.4 μm (2940 cm^{-1}) band is not consistent with the fingerprint of simple hydrocarbon molecules, including polycyclic aromatic hydrocarbons, but it does compare well with the profile of saturated aliphatic

[1] Institut für Experimentalphysik II, Ruhr-Universität Bochum, D-44780 Bochum, Germany; ek@ep2.rub.de.
[2] Institute of Physics, P.O. Box 57, CS-11001 Beograd, Serbia-Montenegro.
[3] Space Science and Astrobiology Division, Mail Stop 245-3, NASA Ames Research Center, Moffett Field, CA 94035.

hydrocarbons with chain lengths of $n = 4–5$ and a CH_2/CH_3 ratio of $\sim$2.5. It is likely that this band represents more than 4% of the total available interstellar carbon (Sandford et al. 1991; Pendleton et al. 1994; Sandford et al. 1995; Pendleton 1997b, 2004). Laboratory spectra of analog materials are important in the interpretation of astronomical infrared data. Questions remain as to the evolution and origin of the organic component of the dense and the diffuse ISM, as material must cycle between these regions as star formation occurs. Here we present new laboratory results from carbonaceous nanometer-sized grains that contribute to our understanding of the evolution of interstellar dust.

Pendleton & Allamandola (2002) have identified a set of criteria based upon the infrared spectra of diffuse interstellar dust that analog laboratory candidates must meet in order to be consistent and, therefore, good interstellar matches. They have shown that although organic materials, in general, exhibit a reasonably good match to the interstellar 3.4 μm band, comparisons of the complete 2–10 μm spectral region between interstellar observations and laboratory-analog data can significantly narrow the possible matches of many proposed ISM analogs. These criteria include spectral profile information for the 2940 cm^{-1} (3.4 μm) band, the abundance of water and carbonyl (largely absent in the interstellar spectra), and the ratio of the CH deformation bands at longer wavelengths ($\sim$6.8 and 7.2 μm) to the 3.4 μm band. The ruling out of possible laboratory candidates is closely tied to the ruling out of certain processes that were once thought relevant to the production of the DISM hydrocarbons. Namely, irradiated ices do not produce 2–10 μm spectra that meet the criteria deduced from the DISM observations, whereas plasma processes, in general, do.

In this paper, we present infrared spectra resulting from our first experiments with spherical particles polymerized in hydrocarbon (acetylene) plasmas with argon or nitrogen as a carrier gas. The particles are analyzed in situ during their growth by means of a sensitive multipass Fourier transform infrared (FTIR) technique. This in situ diagnostic enables us to investigate the formation of particles in a well-defined environment and further investigate the nature of dust in the ISM. Thus, the influence of oxygen and nitrogen on the IR spectra can be studied in detail simply by admixing these gases in a controlled way within the plasma reactor. As a precursor gas, acetylene (C_2H_2) undergoes instantaneous polymerization (Kobayashi et al. 1974) in the plasma, thus enabling very efficient and reproducible dust growth (Kovačević et al. 2003). C_2H_2 has been suggested as a precursor for dust formation in the circumstellar medium, for example, as a possible origin for the formation of polycyclic aromatic hydrocarbons that may take place in the carbon-rich circumstellar shells (Allamandola et al. 1989). Our method is simple and allows different in situ measurements of the nanoparticles, including in situ optical measurements (e.g., scattering, extinction).

This paper is organized in the following way: Section 2 presents the experimental setup. The characteristics of particles grown in an argon-acetylene gas mixture (Kovačević et al. 2003) are described in § 3. A comparison of our lab data with astronomical data is given in § 4. In § 5, the influence of nitrogen on the absorption features of plasma-polymerized particles is discussed. Results are summarized in § 6. Following Pendleton & Allamandola (2002), the astronomical data used for comparison are ground-based near-infrared spectral observations of the 3.4 μm absorption band detected in DISM dust toward Cygnus OB2 No. 12 (an IR-bright background source; Sandford et al. 1991) and the Galactic center (Pendleton et al. 1994), and the mid-infrared absorption spectra of DISM dust observed toward the Galactic center by the *Infrared Space Observatory* (Chiar et al. 2000).

2. EXPERIMENTAL SETUP

The investigations were performed in a capacitively coupled parallel-plate reactor, symmetrically driven by radio-frequency (RF) power at 13.56 MHz. The electrode system consists of two plain stainless steel electrodes, 30 cm in diameter, which are separated by 8 cm. The reactor was operated at room temperature, with a mixture of acetylene, argon, and nitrogen or oxygen gas. The continuous gas flow was governed by mass flow controllers. The total gas pressure was about 0.1 mbar. The characteristic pumping speed of the system gives a mean gas residence time of about 1 minute. The applied RF power was 10–50 W. Details of the experimental setup are given elsewhere (Kovačević et al. 2003).

Infrared absorption spectroscopy was used to monitor the formation of dust particles inside the plasma volume. The particles grow in the bulk plasma between the two electrodes as a result of homogeneous gas-phase nucleation. Since the particles in the plasma were negatively charged, they were confined in the bulk plasma because of the action of the electric force: that is, they levitated between the electrodes without touching the electrodes (previously described in Kovačević et al. 2003; Berndt et al. 2003). The IR beam from a commercial Bruker FTIR spectrometer was directed through KBr windows in the plasma chamber and was focused with an off-axis gold mirror onto an external liquid-nitrogen–cooled HgCdTe detector. The IR beam was allowed to shine through the midplane between the electrodes (without contact with the electrodes or walls) so that it could only "see" the dust particles that were levitating between the electrodes. By means of a multipass technique, we were able to change the optical path length in the plasma from 0.6 m (two passes through plasma reactor) to 7.2 m (24 passes). The cross section of the beam had a radius of 1 cm. Because of the reflections of the beam in the multipass reflection cell, the final area monitored by the IR scan had a size of 2 cm $\times$ 5 cm.

The formation of thin films on windows and mirrors, which could lead to unwanted absorption of the IR beam, was avoided by using an Ar (optionally N_2) gas shower. The unwanted absorption bands were checked by recording background spectra; that is, spectra were measured without plasma and dust particles before and after each measurement session.

A single IR scan could last up to 1 s. Usually we integrated over 50 single scans in order to achieve high resolution in the spectra. We followed the time evolution of the IR signal by measuring full FTIR spectra with a time resolution of 1 minute. In addition to FTIR spectroscopy, dust formation in the discharge was monitored by means of plasma ion mass spectroscopy (details in Kovačević et al. 2003; Stefanović et al. 2003).

During the measurement, there was a significant deposition of DLC (diamond-like carbon) films on the electrodes and discharge chamber walls. Therefore, we cleaned the discharge chamber with oxygen after each measurement session. After this treatment the plasma vessel was pumped for several hours. The residual gas pressure was 6×10^{-6} mbar.

3. CHARACTERISTICS OF THE PLASMA-POLYMERIZED CARBONACEOUS MATERIAL

The growth process of carbonaceous dust particles from the gas phase in bulk plasma has been described by Perrin &

Hollenstein (1999), although some details are still not completely understood. In general, the initial growth of primary clusters (atoms and ions) up to a critical size and concentration is followed by a growth of the dust nuclei as a result of avalanche condensation, which yields small particles, with a radius of a few nanometers. Coagulation and agglomeration of these so-called protoparticles results in isolated negatively charged particles that are a few tens of nanometers, which then further grow by condensation of monomer neutrals, ions, and radicals (accretion). Confinement in the plasma results from their negative charge. The dynamics of the additional growth, involving a periodic growth and loss of particles, is discussed briefly in § 3.3 and in detail in Berndt et al. (2003), Kovačević et al. (2003), and Stefanović et al. (2003). The gas temperature in our chamber was about 300 K. The temperature of the particles was between 300 and 600 K, based upon particle temperature measurements reported by Daugherty & Graves (1993), Praburam & Goree (1995), and Swinkels et al. (2000).

3.1. *TEM/SEM Imaging of the Plasma-polymerized Carbonaceous Material*

Figure 1 shows a scanning electron microscope (SEM) image of a cauliflower-shaped particle with fractal surface texture collected 20 minutes after the ignition of the Ar-C_2H_2 plasma. The particle radius is about 150 nm. The maximum achieved radius at the end of one growth cycle is about 300 nm. The growth speed in the accretion phase is thus about 20 nm per minute.

Spheroidal grain shape and fractal surface texture have been observed in several kinds of dusty plasmas (Haaland et al. 1994; Garscadden et al. 1994), ranging from submicron to submillimeter size scales. The size and structure of the spheroids allows us to conclude that accretion has been the dominant growth mechanism during the growth phase in which the sample was taken. Haaland et al. (1994) explain such a microstructure as columnar growth by ballistic deposition during the accretion phase, which is also the dominant growth mechanism for dust particles in some astrophysical environments.

However, we note that in the very early growth phase of plasma-produced particles, the material properties and the growth texture may be different (Gebauer et al. 2002), allowing for possible core crystallinity. Transmission electron microscope (TEM) measurements performed so far show an amorphous structure to the particles. Because of the limited resolution of the TEM, the presence of a crystalline core or small crystalline islands within the particles cannot be excluded. In general, amorphous carbon materials consist of two intermixed phases (see e.g., Robertson 1991): sp^2, π-bonded clusters, which control the electronic structure and optical properties of the material, embedded in an sp^3-bonded matrix. The latter component consists of a highly cross-linked network of sp^3 sites in a hard *a*-C:H material and a more hydrogenated and polymeric phase in soft *a*-C:H materials.

Measurements performed in a capacitively coupled discharge containing a mixture of argon and methane have shown that the refractive index of spheroidal dust particles (diameter 320 nm) is similar to the refractive index of soft-polymer *a*-C:H materials (Gebauer et al. 2002) rather than that of hard *a*-C:H materials.

3.2. *Mass Spectroscopy Investigations*

The presence of positive ions that may play an important role during the accretion phase has been measured by means of plasma ion mass spectroscopy. The complicated chemistry of a nonequilibrium low-temperature plasma, characterized by a high (20,000 K) electron temperature, and rather low (room) temperatures of ions and neutrals, is illustrated by the mass spectrum of positive ions. The spectrum (Kovačević et al. 2003; Stefanović et al. 2003) reveals the formation of higher mass hydrocarbon cations (up to $m/e \sim 250$) corresponding to hydrocarbons containing up to 18 carbon atoms. In the plasma ion mass spectra, we primarily observe hydrocarbons with an even number of carbon atoms, that is, highly unsaturated hydrocarbons $C_{2n}H_m$. The most abundant positive ions (other than the ions coming from acetylene, as C_2H) are C_4H_2, C_4H_3, C_6H_2, C_6H_4, C_6H_5, C_8H_2, C_8H_3, and C_8H_4 (see Kovačević et al. 2003). We assume that the observed cations originate from highly unsaturated hydrocarbon chains (with approximately 1–5 H per ion even for the higher masses) and aromatic compounds (e.g., masses 76, 77, 78).

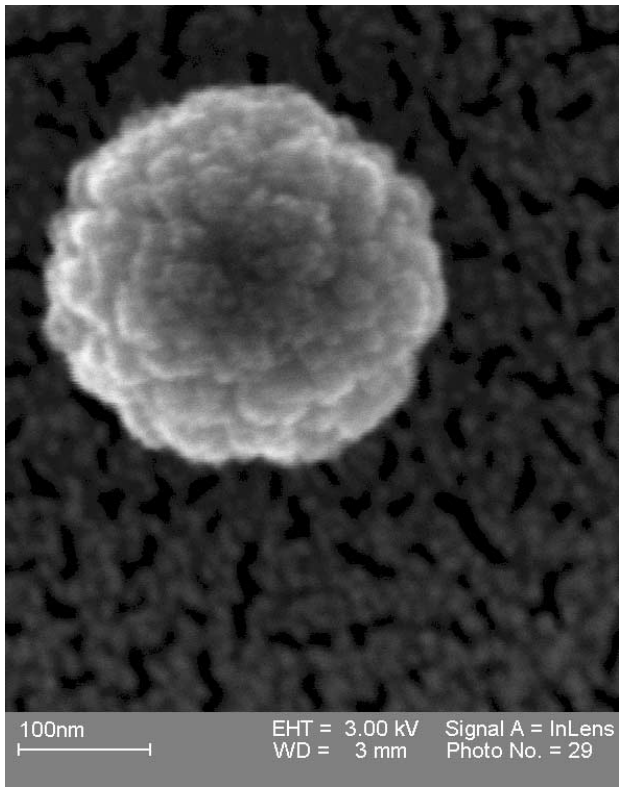

FIG. 1.—SEM image of a plasma-polymerized nanoparticle collected 20 minutes after the beginning of the growth cycle. The particle diameter is about 300 nm. The plasma discharge conditions were Ar : C_2H_2 = 8:0.5 sccm, gas pressure 0.1 mbar, RF power ~15 W.

3.3. *Identification of the Mid-IR Spectra from the Plasma-polymerized Carbonaceous Material*

Figure 2 shows two FTIR spectra in the wavenumber region between 500 and 6500 cm^{-1}. The measurements presented in this figure were obtained 8 minutes and 35 minutes, respectively, after ignition of the discharge. Compared with the spectrum of the gas mixture (Ar:C_2H_2 = 8:0.5 standard cubic centimeters per minute [sccm]; Berndt et al. 2003; Kovačević et al. 2003) measured before the plasma was switched on, these spectra exhibit completely different shapes. The most obvious difference is the strong increase in the absorbance at high frequency. This effect can be attributed to Rayleigh scattering and is a global indication of the presence of submicron-sized dust particles in the reaction chamber. The wavelength dependence in the case of Rayleigh scattering is described by a λ^{-4} dependence. The scattering

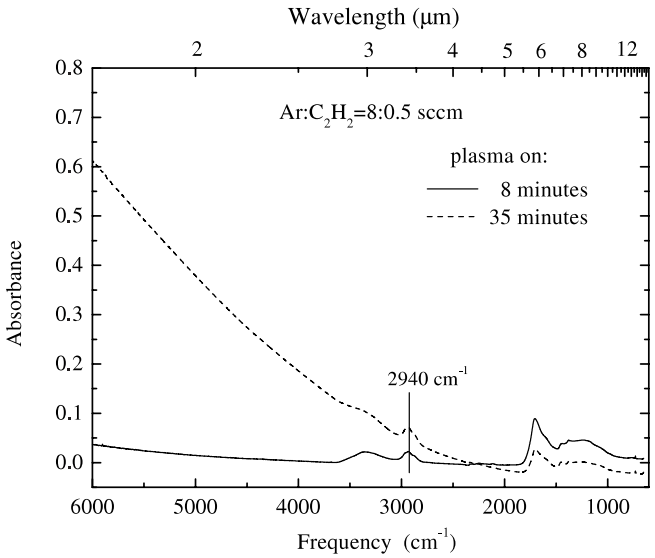

FIG. 2.—In situ FTIR spectra of carbonaceous dust particles polymerized in an Ar-C_2H_2 plasma (Kovačević et al. 2003) in the range 6000–600 cm^{-1}. The solid line shows a measurement performed 8 minutes after the plasma was switched on; the dashed line shows a measurement after 35 minutes. Discharge conditions: Ar:C_2H_2 = 8:0.5 sccm, gas pressure 0.1 mbar, RF power 15 W. The absorbance shows a strong increase toward higher wavenumbers, which can be attributed to Rayleigh scattering. This scattered signal is a global indication of the presence of dust particles in the reaction chamber.

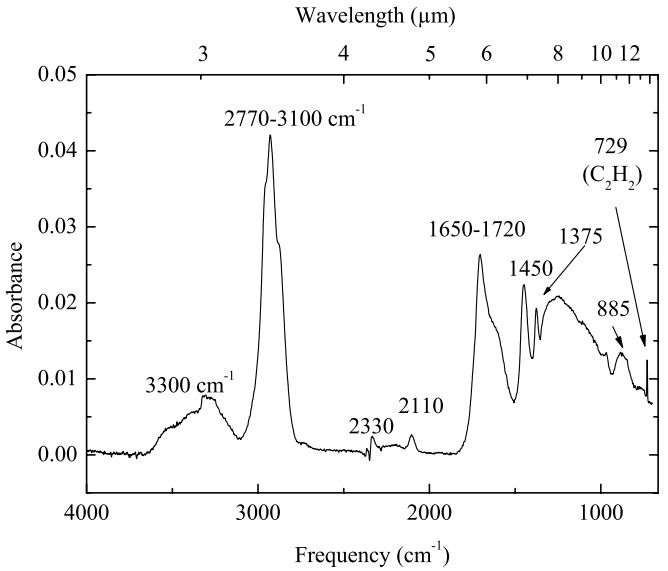

FIG. 4.—Infrared fingerprint of the plasma-polymerized dust in the range 4000–700 cm^{-1} after baseline correction (obtained after 90 minutes, particle radius 150 nm). Discharge conditions: Ar:C_2H_2 = 8:0.5 sccm, gas pressure 0.1 mbar, RF power 15 W. The wavenumbers of the most prominent bands are given in cm^{-1}.

intensity was used to trace the relative growth of the particles. Figure 3 shows the temporal evolution of the absorbance at 5000 cm^{-1} as a function of time. The periodic behavior of the absorbance can be explained by a simple model.

The negatively charged particles are confined in the plasma potential as long as the different forces acting on a single particle are balanced. Since these forces—including the electric force, the ion drag force, the neutral drag force, the force caused by thermophoresis, and the gravitational force—scale with different powers of the particle radius, the confinement of the particles strongly depends on their size. As soon as the particles reach a critical size, they are dragged out of the bulk plasma by the ion drag force, or they fall toward the lower electrode because of the gravitational force. Then a new growth cycle starts.

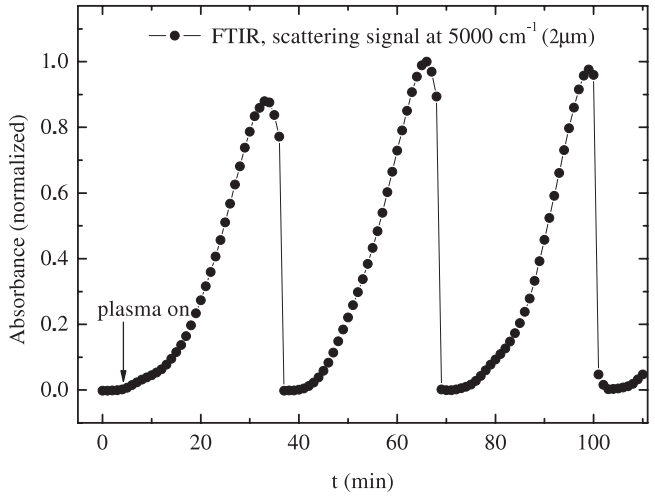

FIG. 3.—Evolution of the absorbance at 5000 cm^{-1} (2 μm) as a function of time. The signal at this high frequency can be attributed to Rayleigh scattering and is a global indication of the presence of submicron-sized dust particles in the reaction chamber. One can observed how the particle formation process starts: the increase of the curve is due to an increase in particle size, and the decrease corresponds to particle disappearance from the bulk plasma (particles with critical size being pushed out of the plasma).

In addition to Rayleigh scattering, the FTIR spectrum exhibited several new absorption bands as soon as the plasma was switched on. Comparison of these spectra with results from ex situ FTIR measurements on particles extracted from the discharge (Stoykov et al. 2001) indicates that the absorption bands can be attributed to nanoparticles grown in the plama.

The absorption features correlated with the nanoparticles in the bulk plasma (features observable only in the presence of dust) remain unchanged with respect to peak position and profile shape from the initial observation (particles sizes of about 50 nm) to the end of one growth cycle (about 600 nm diameter particles grown in Ar plasma), and the specific features repeat in every growth cycle. The increase in strength is likely due to the change of the particle size during one growth cycle (the density of the particles levitating in the discharge can be supposed constant in the accretion phase, as the SEM investigations show monodispersivity of the collected particles).

The complicated signature of the FTIR spectrum becomes more obvious after a baseline correction (Fig. 4) is made. (The spectrum in Fig. 4 was obtained after 90 minutes, corresponding to a particle size of 150 nm in radius.) In our case, a sufficient baseline correction eliminated the Rayleigh scattering (λ^{-4}, r^6), as our IR beam "sees" only the nanoparticles in the bulk plasma (§ 2).

Numerous aliphatic (mostly sp^3) bonds are detected: CH_3 symmetric bending modes at 1375 $\pm$ 5 cm^{-1}, CH_3 asymmetric bending (deformation) modes at 1450 $\pm$ 20 cm^{-1}, and a very strong triple peak at 2770–3100 cm^{-1} (—CH_3 symmetric stretching modes [2870 cm^{-1}] and asymmetric modes [2960 cm^{-1}], and —CH_2— asymmetric stretching modes [2926 cm^{-1}]). This triple peak correlates with the 3.4 μm feature observed in astronomical spectra in the DISM. Hereafter, we will adopt the term used in the astronomical literature and call this peak the 3.4 μm band, reflecting the general central peak position.

The presence of triple C≡C bonds is also indicated, by the weak, sharp absorption peak at 2110 cm^{-1} (C≡C stretching of monosubstituted acetylene). The nearby peak at 2330 cm^{-1}

originates from traces of carbon dioxide and is due to the C=O asymmetric stretching vibrations. The absorption band at 3300 cm^{-1} that was attributed to the ≡C−H stretching mode of monosubstituted acetylene by Stoykov et al. (2001) is, in our case, a broad band, and we attribute this band to the presence of trapped water/OH stretching vibrations (Günzler & Heise 1996; Elyashevich 2000; Socrates 1980), common in many laboratory-produced analog materials (Pendleton & Allamandola 2002). In our spectra, the sharp ≡C−H feature may be lost within this broad and strong OH band. In fact, it has been speculated that the presence of water ice in dense-cloud dust obscures the C−H stretch feature that might otherwise be seen there. Mennella et al. (1999) have offered an interesting alternative, which demonstrates that the ice layer likely prevents reformation of the C−H band after it is destroyed by energetic processes such as UV photon or cosmic-ray bombardment.

The peak at 1604 cm^{-1}, appearing as a shoulder within the broad peak between 1500 and 1730 cm^{-1}, is characteristic of aromatic C=C stretching vibrations. The presence of aromatic compounds is strongly confirmed by weaker peaks observed at 757, 851, and 885 cm^{-1}, which originate from C−H deformational vibrations of (differently substituted) aromatic hydrocarbons (Günzler & Heise 1996; Elyashevich 2000; Socrates 1980). The =C−H stretching band at 3030 cm^{-1}, which is nearly overshadowed by the strong, broad bands near 2900 and 3300 cm^{-1} (the latter being connected to trapped water), has either an aromatic or an alkene origin (Duley & Grishko 2003).

The strong peak between 1500 and 1730 cm^{-1} can be attributed to carbonyl C=O stretching vibrations (Günzler & Heise 1996; Elyashevich 2000; Socrates 1980). The latter results from the oxidation of carbon, caused either by water contamination or by oxygen that has been deliberately added (Socrates 1980; Arnoult et al. 2000). To confirm this assumption, we added a small amount of oxygen to our gas mixture, and these results are discussed in the following section.

In addition to the carbonyl C=O stretching vibrations, the broad band between 1500 and 1730 cm^{-1} contains δOH (a deformational vibration at about 1640 cm^{-1} corresponding to the OH stretching vibration around 3300 cm^{-1}) and C=C stretching bands. The OH deformation and C=C stretching band are blended into a shoulder of the strong carbonyl band.

4. PLASMA-POLYMERIZED DUST AS AN ISM ANALOG

Dust in the ISM at temperatures of 10–30 K shows clear evidence of organic solid-state bands in the 2–10 μm region, arising from C, H, O, and N. Dust cycles between the dense-cloud regions ($n \sim 10^6$–10^8 cm^{-3}), where ices and energetically processed material reside, and the DISM ($n \sim 1$–100 cm^{-3}), where the aliphatic C−H band originates (Chiar et al. 1998; Pendleton & Allamandola 2002; Mennella et al. 2004). The 5–8 μm region of the interstellar spectrum, which is so critical for diagnostic use, is not observable from the ground, because of atmospheric interference. The *Infrared Space Observatory* (*ISO*) did obtain data in this region for dust seen toward the luminous Galactic center (Chiar et al. 2000), which is dominated by DISM dust. Pendleton & Allamandola (2002) have combined the information contained in this spectrum with weaker (but consistent) indications from an alternate DISM line of sight toward Cyg OB2 No. 12 using data from the Kuiper Airborne Observatory (Pendleton 1997a) and *ISO* (Whittet et al. 1997). We evaluate our candidate analog material as proposed in the literature (Pendleton & Allamandola 2002) using the four spectral characteristics based upon interstellar data developed therein:

1. Comparison of the profile and subpeak positions of the 2940 cm^{-1} (3.4 μm) feature;
2. The ratio between the optical depth/absorption intensity of the 2940 cm^{-1} (3.4 μm) CH stretch feature and the CH deformation modes at 1450 and 1375 cm^{-1} (6.89 and 7.25 μm);
3. Optical depth of the carbonyl group at 1700 cm^{-1} (5.89 μm); and
4. The presence of water (OH stretching vibrations) at 3300 cm^{-1} (3.03 μm).

It should be noted that in astronomical data on the DISM, characteristics 3 and 4 are either not observed or are very weak, providing strong upper limits on acceptable amounts in laboratory candidate spectra.

According to Pendleton & Allamandola (2002), each of these criteria is an essential spectral constraint. If one of these criteria is not fulfilled, the corresponding analog material cannot be considered a suitable astrophysical analog given the observational data available so far. Duley & Grishko (2003) showed, for example, that the feature at 3.4 μm can be reproduced by a great variety of carbon-containing materials. The authors showed that the feature of the 3.4 μm band of the substituted paraffin molecules 6,9,12-tripropyl heptadecane ($C_{25}H_{54}$) and 2,6-dimethyl undecane ($C_{13}H_{28}$) has a striking similarity to that of the DISM band at 3.4 μm, although neither molecule is likely to be the source of the interstellar 3.4 μm absorption.

These examples demonstrate that the important feature at 3.4 μm, which is discussed in § 4.1 in more detail, has to be considered together with the other criteria given above to have astrophysical relevance. *Spitzer Space Telescope* observations will be key to further investigations, although the spectral resolution in this critically diagnostic 5–8 μm region is quite low. Further mission concepts such as the *Astrobiology Explorer* (Ennico et al. 2003) will have optimized abilities in this region.

Another (quantitative) criterion to consider concerns the mass absorption coefficient in the 2950 cm^{-1} band, as suggested by Furton et al. (1999). Assuming that 80 parts per million (ppm) of carbon relative to hydrogen is depleted from the gas phase to form solid carbonaceous material, the authors claim that any laboratory analog should have a C−H stretch peak mass absorption coefficient higher than about 10^3 cm^2 g^{-1}. Based upon investigations that show a relation between the mass absorption coefficient and the H/C ratio of hydrogenated amorphous carbon (HAC) materials, the authors further concluded that a mass absorption coefficient of 10^3 cm^2 g^{-1} requires an H/C ratio greater than 0.5. The HAC material presented by Furton et al. (1999) has values of 1400 cm^2 g^{-1} and H/C = 0.5. With this intrinsic strength, almost all of the available solid carbon would be locked up in such HAC material (Furton et al. 1999).

Locking up all the carbon in HAC grains poses a general problem for models of interstellar dust, since there are other spectral characteristics of the interstellar extinction curve that are generally attributed to carbonaceous dust. In particular, the 2175 Å bump that dominates the far-UV extinction curve is ascribed to the π-π^* transition in small (200 Å) aromatic carbon dust grains, and some 100 ppm of the C is needed to explain the observed strength of this band with such materials. Following Schnaiter et al. (1998), one way to resolve this issue is to have the 2175 Å bump and the 3.4 μm band be carried by the same amorphous carbon grains, with the 3.4 μm band originating in the sp^3 component while the 2175 Å bump stems from the sp^2-bonded component. It is clear that further studies of plasma polymerization–produced materials in the far-UV may be very illuminating for this question, but we defer this to a future publication.

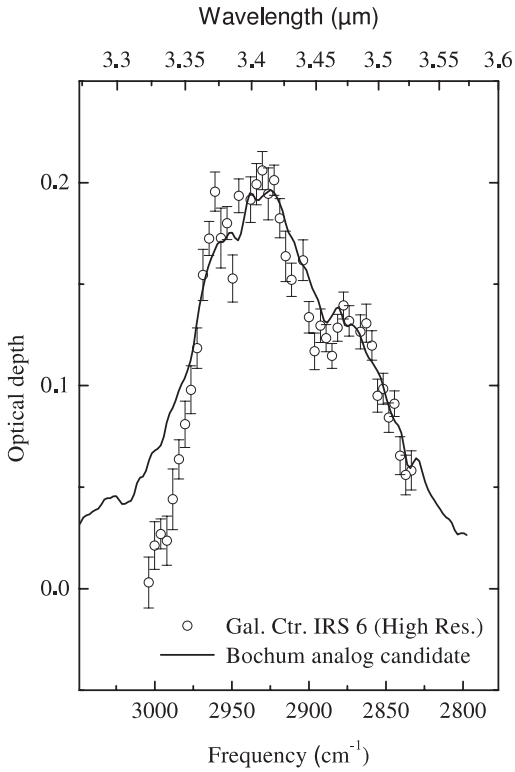

FIG. 5.—Comparison of the 2940 cm^{-1} (3.4 μm) feature: *solid line*, the laboratory dust (Kovačević et al. 2003); *circles*, Galactic center IRS 6. The data for the laboratory polymerized dust were multiplied by a factor of 16 in order to match the optical depth of the Galactic center data. The astronomical data are taken from Pendleton & Allamandola (2002).

4.1. *Hydrocarbon Stretch Feature*

The strongest feature observed in our spectra is that at 2940 cm^{-1} (3.4 μm), which is well matched in peak position, profile, and relative strengths to the CH_2 and CH_3 groups detected at 3.4 μm in the DISM. Figure 5 shows a comparison of this feature from our plasma-polymerized dust with the astronomically detected absorption data measured toward the Galactic center source IRS 6E (Pendleton et al. 1994).

Substructures in the 2940 cm^{-1} (3.4 μm) feature are identified as $-CH_3$ symmetric stretching (2870 cm^{-1} [3.48 μm]) and antisymmetric $-CH_3$ (2960 cm^{-1} [3.38 μm]) and $-CH_2-$ stretching (2926 cm^{-1} [3.42 μm]) (Sandford et al. 1991). The relative strengths of these subfeatures imply a $-CH_2/-CH_3$ ratio of $\sim$2.5, characteristic of short-chain hydrocarbons (Sandford et al. 1991; Pendleton et al. 1994; Pendleton & Allamandola 2002). The details of the profile are explained in the literature, including a signature of possible perturbing electronegative groups that can blend some of the subfeatures seen in normal alkanes (Sandford et al. 1991). Although once thought to originate in dense-cloud dust, where photoprocessed organic mantle material residing on ice-covered silicate cores could reasonably be expected (Greenberg 1982; Sandford et al. 1991; Pendleton et al. 1994; Greenberg et al. 1995; Greenberg & Li 1996), the 3.4 μm absorption band has not yet been seen along dense-cloud lines of sight where ices exist (Allamandola et al. 1992; Brooke et al. 1999; Pendleton & Allamandola 2002). The distinctive signature of the 3.4 μm aliphatic band hydrocarbons should be detectable even under an ice mantle (Baratta & Strazzulla 1990), so explanations for its absence have been sought through physical destruction mechanisms (Mennella et al. 1999), and the observational search continues along quiescent sight lines of dense-cloud ice (Pendleton 2004). The small peak in laboratory spectra visible shortward of the 3.4 μm feature, at 3030 cm^{-1} (3.3 μm), arises from the $=C-H$ stretch from either aromatic or aliphatic (alkene) hydrocarbons. Such absorption has been tentatively claimed in the interstellar data in diffuse and dense dust clouds (Pendleton et al. 1994 and Brooke et al. 1999, respectively).

4.2. *Ratio between* CH *Stretching and Deformation Modes*

As shown in Pendleton & Allamandola (2002), a comparison between the optical depths of the 3.4 μm stretching groups and the deformation (bending mode) bands at 6.8 and 7.2 μm in the DISM reveals a strong dominance of the stretching bands. In our spectra, we observe CH deformation bands as two peaks at 1375 cm^{-1} (weaker) and 1450 cm^{-1} (stronger), in addition to the absorbance of the CH stretching band. The latter is stronger than the absorbance of the deformation bands, revealing the largely alkane nature of the material (as is the case for many other hydrocarbon materials, such as HAC analogs). In this way, the IR spectra of our dust particles satisfy a critical condition suggested by Pendleton & Allamandola (2002) for a "good" analog material.

4.3. *Presence of Carbonyl and* OH *groups in IR Spectra*

Analysis of the IR spectra of our particles shows clear OH stretching vibrations around 3300 cm^{-1}, as well as a strong carbonyl band at 1700 cm^{-1}. These bands originate from impurities (oxygen or water) that are present in the discharge chamber. The concentration of these impurities can be decreased by running the discharge for several hours (Kovačević et al. 2003). This was confirmed by time-resolved FTIR measurements. Figure 6 shows three fingerprint spectra taken at 20, 53, and 87 minutes after the discharge was switched on. The spectra are normalized to the absorption line at 2940 cm^{-1}. Clearly, the relative intensities of the peaks at 1250, 1700, and 3300 cm^{-1} decrease with time compared with those at 1375, 1450, and 885 cm^{-1}. We stress, however, that the presence of $C=O$ is

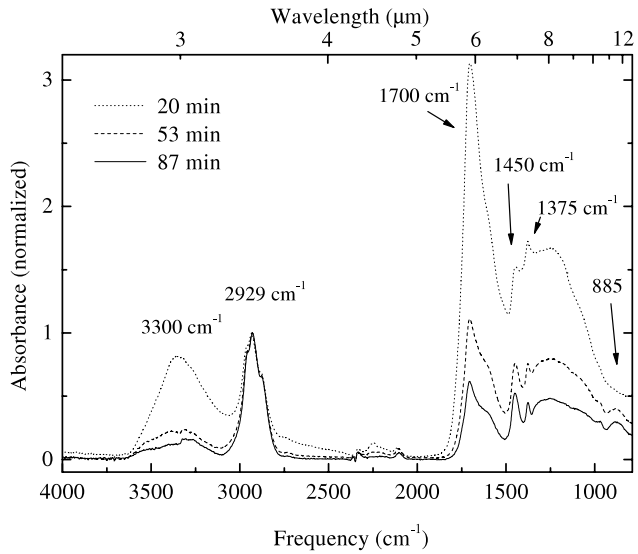

FIG. 6.—Infrared fingerprint spectra of the dust polymerized in low-pressure discharge in the range 4000–780 cm^{-1} taken 20 minutes (*dotted line*), 53 minutes (*dashed line*), and 87 minutes (*solid line*) after the discharge was switched on. All data are normalized to the 2940 cm^{-1} (3.4 μm) feature. The discharge parameters were the same as in the previous figures.

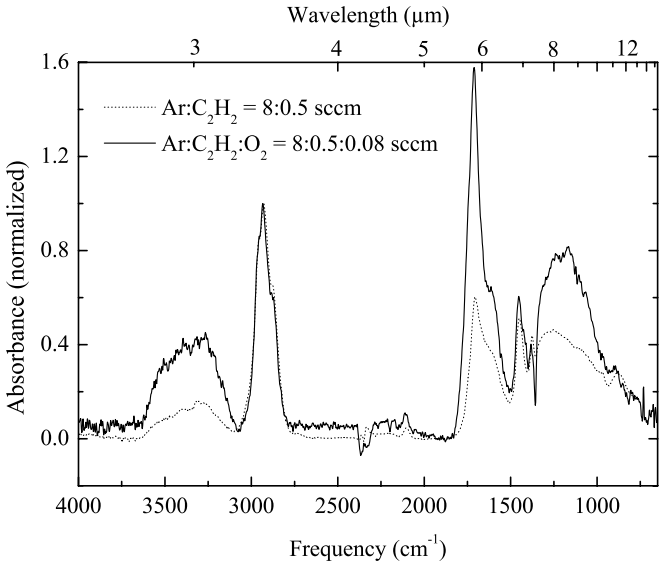

FIG. 7.—Influence of oxygen admixture on the IR spectra of plasma-polymerized dust particles: *dotted line*, spectrum of dust particles grown in an $Ar:C_2H_2 = 8:0.5$ sccm gas mixture; *solid line*, spectrum of dust particles grown in an $Ar:C_2H_2:O_2 = 8:0.5:0.08$ sccm mixture. The total gas pressure for both mixtures was 0.1 mbar, and the discharge power was 15 W.

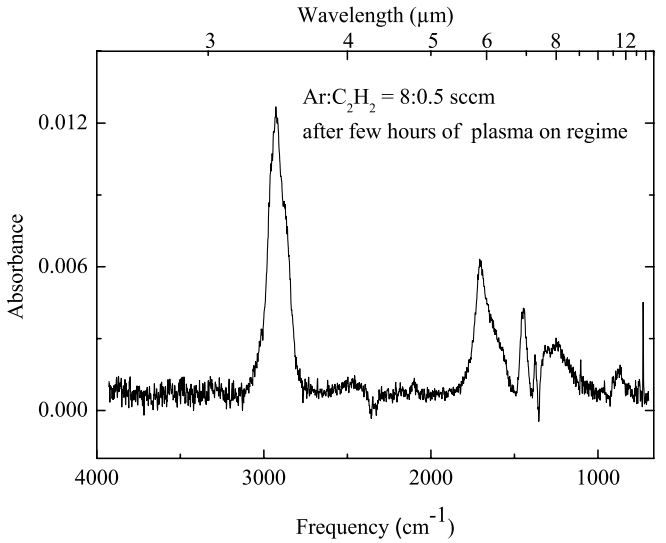

FIG. 8.—Infrared fingerprint spectrum of the plasma-polymerized dust particles obtained after running the discharge ($Ar:C_2H_2 = 8:0.5$ sccm, 0.1 mbar, 15 W) for several hours. The spectrum shows the gradual disappearance of the observable oxygen and water content, e.g., in the decrease of the 3300 cm^{-1} (trapped water) and 1700 cm^{-1} (carbonyl) absorption bands.

harder to eliminate from the spectra than that of water. This reflects the higher intrinsic strength of the absorption band associated with the C=O stretching mode, which makes even small traces of carbonyl groups detectable.

This trend can be reversed by adding oxygen to the discharge chamber, as shown in Figure 7. Even very small amounts of oxygen (0.08 sccm) result in a strong increase in the strength of the carbonyl band, the appearance of a strong band between 1000 and 1300 cm^{-1}, and a strong, broad feature between 3600 and 3000 cm^{-1} due to the OH stretching band. The presence of OH groups and more prominent C=O stretching vibrations are also indicated by an increase of the 1510–1730 cm^{-1} shoulder. Trapped CO is apparent at 2138 cm^{-1} (4.67 μm). The presence of electronegative groups can also change the intensity of the subfeatures in the dust fingerprint. Considering that the intrinsic strength of the hydrogen-bonded OH stretch and carbonyl C=O stretch is up to 10 times stronger than the intrinsic C—H stretch (Pendleton & Allamandola 2002; Socrates 1980), these groups can be detected even if their concentration is relatively small. Consequently, the addition of a very small amount of oxygen is sufficient for these bands to appear.

Switching off the oxygen supply results in the full restoration of the fingerprint discussed earlier. With this understanding of our discharge, we were able to obtain IR spectra that better satisfy the interstellar criteria 3 and 4, simply by running the discharge for several hours (Fig. 8).

The presence of unsaturated hydrocarbon bonds becomes visible as a sharp peak at 3015 cm^{-1}, or 3.31 μm (shoulder of the strong 2940 cm^{-1} feature), when the amount of water decreases (Fig. 9). In Figure 5, this peak was broader and was shifted by +15 cm^{-1}, perhaps as a result of the strong presence of electronegative groups in the material. The shift of the center of the band to longer wavelengths is rather typical for H—C= aliphatic modes, and the shift confirms the identification of this peak as alkene rather than aromatic in origin (Grishko & Duley 2003).

Finally, although the carbonyl band is not yet completely eliminated, it is much weaker, and the shoulder now reveals a band centered at 1580 cm^{-1}. We identify the latter with the C=C skeletal vibrations of the sp^2 aromatic clusters present in the material.

5. THE EFFECT OF NITROGEN ON THE INFRARED SPECTRA

The existence of nitrogen in both gas and solid phase is clearly seen in observational IR spectra, especially in dense molecular

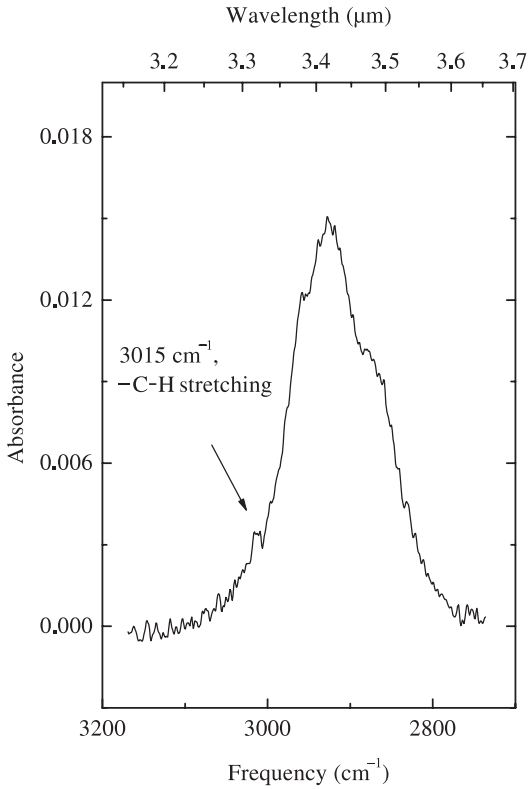

FIG. 9.—Magnification of the 2940 cm^{-1} (3.4 μm) feature from Fig. 7, showing the presence of alkene compounds at 3015 cm^{-1} in the IR spectra obtained few hours after the discharge was switched on. This shoulder on the 3.4 μm feature is shifted by about −15 cm^{-1} compared with Figs. 4–6. Discharge conditions: $Ar:C_2H_2 = 8:0.5$ sccm, 0.1 mbar, 15 W.

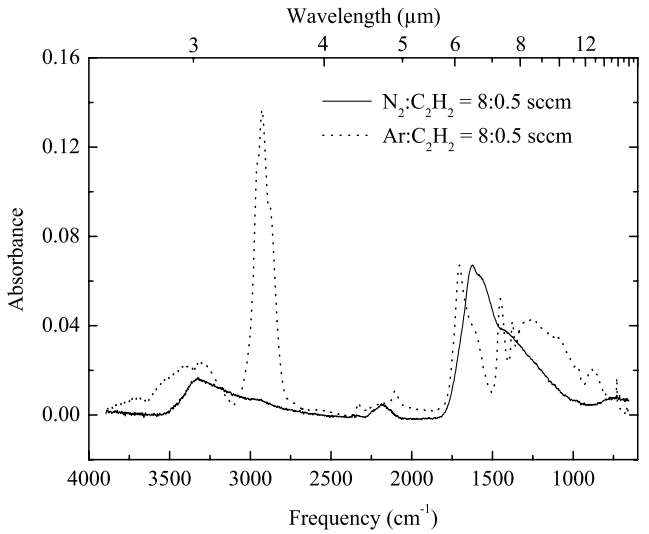

FIG. 10.—Influence of nitrogen admixture on the IR spectra of plasma-polymerized dust particles: *dotted line*, $Ar:C_2H_2 = 8:0.5$; *solid line*, $N_2:C_2H_2 = 8:0.5$ sccm (total pressure 0.1 mbar, RF power 15 W).

clouds, where interstellar ices form. The spectral feature at 4.62 μm (solid phase; Lacy et al. 1984; Pendleton et al. 1999; Chiar et al. 2000; Whittet et al. 2001; Demyk et al. 1998; Goto et al. 2003) is associated with a CN group (XCN), which is most likely the OCN^- band detected in laboratory experiments (Schutte et al. 1997; Palumbo et al. 2000). In the case of the diffuse ISM, however, elemental nitrogen is present in the gas phase with no obvious solid-state component. The XCN band is extremely weak or nonexistent in the DISM, as shown by Whittet et al. (2001), where less than 0.3% of the available elemental nitrogen is in C≡N groups (assuming solar abundance). For example, dust observed toward the dark cloud R CrA IRS 2 reveals less than 0.1% nitrogen in C≡N (Whittet et al. 2001). Nitrogen depletion from the gas phase into the dust in diffuse interstellar clouds was also shown to be very low and insensitive to physical conditions by Meyer et al. (1997), where the interstellar nitrogen abundance in the local Milky Way was found to be about 80% of the solar value. In dense clouds, processing of icy material by cosmic rays or UV photons has been linked to the 4.62 μm XCN band rather convincingly. As the only processed feature detected so far, the role of nitrogen in dense-cloud ices is therefore significant, and we further investigate that here.

To investigate the role of nitrogen in the carbon chemistry of this experiment, we polymerized our carbonaceous particles in gas mixtures containing nitrogen. Figure 10 shows a comparison between the IR spectra of nanoparticles polymerized in an argon-acetylene discharge (as in Fig. 4) and particles polymerized in a mixture of nitrogen and acetylene (same mixing ratio as in the case with argon as a carrier gas, i.e., $8:0.5 = N_2:C_2H_2$, measurement after 9 minutes).

First, in contrast to the spectra resulting from experiments with Ar as the carrier gas, the infrared spectrum from the nitrogen-acetylene discharge is dominated by a strong, broad absorption peak centered at about 1625 cm^{-1} (6.15 μm) (compare with Figs. 4, 6, and 7). According to González et al. (1997) and Ferrari et al. (2003), this peak may be attributed to C=N vibrations, which indicates the presence of nitrogen atoms bonded to the skeleton of the dust particles. This broad peak probably contains superposed weaker NH deformational vibrations and traces of OH, although experiments with H-D substitution in the precursor gas, as shown by Ferrari et al., support C=N as the dominant site.

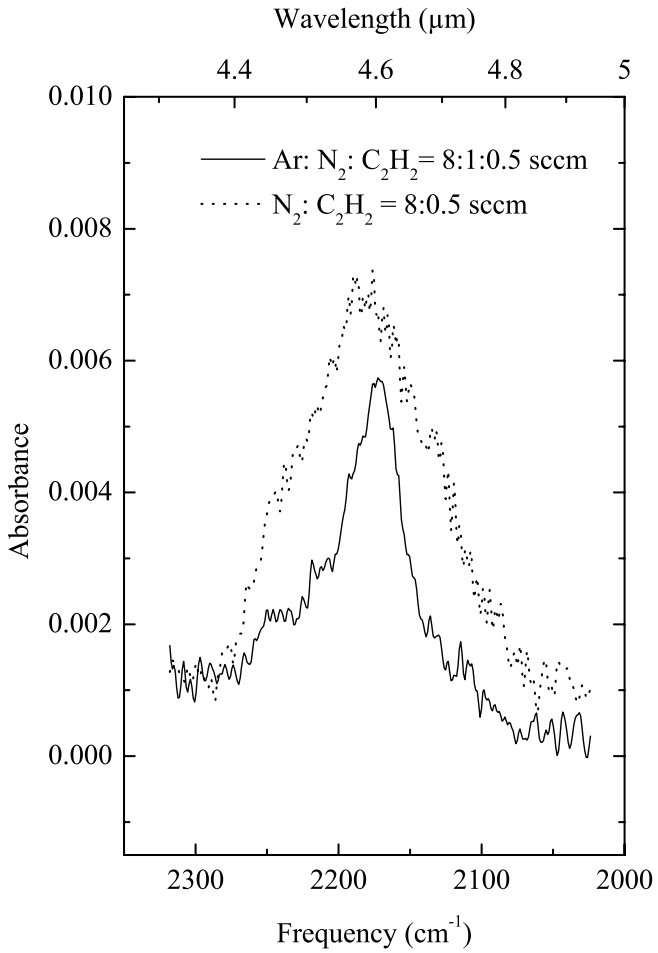

FIG. 11.—Comparison of the 4.62 μm feature of the laboratory polymerized dust particles for different nitrogen amounts (same particle size) in the gas mixture: *dotted line*, $N_2:C_2H_2 = 8:0.5$; *solid line*, $Ar:N_2:C_2H_2 = 8:1:0.5$ sccm (in both cases total pressure 0.1 mbar, RF power 15 W).

Second, there is a strong and broad feature peaking at 3332 cm^{-1} (3.0 μm) in the nitrogen-acetylene discharge spectrum. We can identify this broad peak with NH stretching vibrations from an H—CN band with a very small shoulder at 3.4 μm due to CH stretching vibrations. The presence of OH vibrations due to impurities is possible, but we also observed this strong, broad feature after a few growth cycles when the water/oxygen presence should be minimized (see § 4.3) and therefore conclude that NH vibrations dominate. The striking result is that the main absorption feature at 2940 cm^{-1} (3.4 μm) in the mixtures with nitrogen is drastically weakened in comparison with the HCN bands. This result is similar to the observations in the spectra of HAC analogs prepared in the presence of H_2/N_2 and H_2/NH_3 (Grishko & Duley 2002).

Perhaps a fraction of the carbon and hydrogen that would otherwise produce the 3.4 μm feature goes into making HCN. This raises the intriguing possibility that the absence of the DISM 3.4 μm aliphatic hydrocarbon band in dense-cloud spectra (Allamandola et al. 1992; Pendleton 2004) results from production of the HCN band, which is hidden by the strong 3.08 μm water ice band in dense clouds.

Another broad peak located around 2165 cm^{-1} (4.62 μm) corresponds to the astronomical XCN/OCN^- band seen in dense-cloud ices. Better insight into the shape and position of this peak in plasma-polymerized analogs is given by Figure 11. The figure presents results obtained from two different gas mixtures: the

previously shown nitrogen-rich mixture, $N_2:C_2H_2 = 8:0.5$ sccm (*dotted line*), and a nitrogen-poor mixture, $Ar:N_2:C_2H_2 = 8:1:0.5$ sccm (*solid line*). The peak is broadened in the nitrogen-rich mixture and has its maximum at 2180 cm^{-1}. In the nitrogen-poor mixture, the peak is narrower and the maximum is moved to lower frequencies, 2165 cm^{-1}. The temperature of the gas mixture was about 300 K in both cases. This broad absorption feature can be identified as stretching vibrations of C≡N bonds (Socrates 1980; Pendleton et al. 1999; Palumbo et al. 2000; Chiar et al. 2002; Bernstein et al. 2002). As we cannot completely exclude the presence of impurities (oxygen, water) in our system, this band can be correlated with the presence of either CNO (isonitrile) or NCO (fulminate) groups.

6. CONCLUSIONS

With regard to diffuse ISM dust, the in situ infrared spectra of nanoparticles produced by low-pressure reactive plasma polymerization reveal weak OH and carbonyl stretching bands, strong aliphatic CH stretching bands and correlated weaker CH deformation bands, and traces of aromatic compounds. The experimental IR fingerprint provides a good match to the data obtained from astronomical observations, for example, mid-IR spectra of the DISM (2940 cm^{-1} feature) and near-IR ground-based spectra of interstellar dust as seen along the line of sight toward the Galactic center.

The dominant feature at 2940 cm^{-1} (3.4 μm) from the plasma-polymerized hydrocarbon nanoparticles matches the feature observed from the interstellar dust toward the Galactic center (Galactic center source IRS 6E). The ratio of the associated doublet at 1450 cm^{-1} (6.86 μm) and 1375 cm^{-1} (7.25 μm), identified as C−H deformation modes, to the 3.4 μm stretching band is also consistent with that observed in the interstellar medium.

Further measurements are necessary in order to determine the amount of carbon in our nanoparticles. Complete information about an analog candidate should include measurements in the UV and visible range, as well as the determination of the H/C ratio. Far-UV studies can also address the important question of whether these same particles can also be the carriers of the dominant 2175 Å bump in the interstellar extinction curve.

With regard to dense-cloud dust, the experiment presented here allowed the variation, in a simple and controlled way, of the physical and chemical parameters important for particle formation and the observation of their specific IR fingerprint. Variations in the water/oxygen amount and in the nitrogen bonds present in the spectra resulted, which may have application for dense-cloud ices. In the case of particles grown with nitrogen as a carrier gas, the spectra show strong dominance of nitrogen bands over pure hydrocarbon bands. Future investigations of these carbon nitride nanoparticles will include X-ray photoelectron spectroscopic measurements to determine the nitrogen content within the particles.

Laboratory-polymerized dust with astrophysical characteristics allows one the possibility of performing different in situ optical measurements (Gebauer et al. 2002) and measurements on collective effects of the dust (charging, waves, scattering). Plasma-polymerized carbonaceous particles have a strong potential for further investigations. Our particles are a competitive candidate for laboratory investigations that seek to match the diffuse ISM dust spectra.

We thank an anonymous referee and Professor A. G. G. M. Tielens for very helpful comments that improved the manuscript. The authors also kindly acknowledge R. Neuser for SEM images of our particles. This study was supported by the Deutsche Forschungsgemeinschaft within SFB 591 (B1 and B5). Y. J. P. gratefully acknowledges support for this work from NASA's Exobiology Program (344-38-12-09 and 21-344-58-1P).

REFERENCES

Adamson, A. J., Whittet, D. C. B., Chrysostomou, A., Hough, J. H., Aitken, D. K., Wright, G. S., & Roche, P. F. 1999, ApJ, 512, 224
Adamson, A. J., Whittet, D. C. B., & Duley, W. W. 1990, MNRAS, 243, 400
Allamandola, L. J., Sandford, S. A., Tielens, A. G. G. M., & Herbst, T. M. 1992, ApJ, 399, 134
Allamandola, L. J., Tielens, A. G. G. M., & Barker, J. R. 1989, ApJS, 71, 733
Arnoult, K. M., Wdowiak, T. J., Wade, M. L., Garner, J. R., Beegle, L. W., & Coltress, B. G. 2000, in Lunar and Planetary Science XXXI (Houston: Lunar Planet. Inst.), No. 1472
Baratta, G. A., & Strazzulla, G. 1990, A&A, 240, 429
Berndt, J., Hong, S., Kovačević, E., Stefanović, I., & Winter, J. 2003, Vacuum, 71, 377
Bernstein, M. P., Sandford, S. A., & Allamandola, L. J. 2002, ApJ, 542, 894
Bridger, A., Wright, G. S., & Geballe, T. R. 1994, in Infrared Astronomy with Arrays: The Next Generation, ed. I. S. McLean (Dordrecht: Kluwer), 537
Brooke, T. Y., Sellgren, K., & Geballe, T. R. 1999, ApJ, 517, 883
Butchart, I., McFadzean, A. D., Whittet, D. C. B., Geballe, T. R., & Greenberg, J. M. 1986, A&A, 154, L5
Cassinelli, J. P. 1979, ARA&A, 17, 275
Chiar, J. E., Adamson, A. J., Pendleton, Y. J., Whittet, D. C. B., Caldwell, D. A., & Gibb, E. L. 2002, ApJ, 570, 198
Chiar, J. E., Pendleton, Y. J., Geballe, T. R., & Tielens, A. G. G. M. 1998, ApJ, 507, 281
Chiar, J. E., Tielens, A. G. G. M., Whittet, D. C. B., Schutte, W. A., Boogert, A. C. A., Lutz, D., van Dishoeck, E. F., & Bernstein, M. P. 2000, ApJ, 537, 749
Daugherty, J. E., & Graves, D. B. 1993, J. Vacuum Sci. Technol. A, 11, 1126
Demyk, K., Dartois, E., d'Hendecourt, L., Jourdain de Muizon, M., Heras, A. M., & Breitfellner, M. 1998, A&A, 339, 553
Duley, W. W., & Grishko, V. I. 2003, Ap&SS, 285, 699
Elyashevich, M. A. 2000, Atomnaya i molekulyarnaya spektroskopiya (2nd ed.; Moscow: Ed. URSS)
Ennico, K. A., et al. 2003, Proc. SPIE, 4850, 1149
Ferrari, A. C., Rodil, S. E., & Robertson, J. 2003, Phys. Rev. B, 67(15), No. 5306
Furton, D. G., Laiho, J. W., & Witt, A. N. 1999, ApJ, 526, 752
Garscadden, A., Ganguly, B. N., Haaland, P. D., & Williams, J. 1994, Plasma Sources Sci. Technol., 3, 239
Gauger, A., Gail, H.-P., & Sedlmayr, E. 1990, A&A, 235, 345
Gebauer, G., Hong, S., Galka, T., Berndt, J., & Winter, J. 2002, Europhys. Conf. Abstr., 26B, No. O-5.24
Gehrz, R. D., Truran, J. W., Williams, R. E., & Starrfield, S. 1998, PASP, 110, 3
González, P., et al. 1997, Appl. Surface Sci., 109–110, 380
Goto, M., et al. 2003, ApJ, 589, 419
Greenberg, J. M. 1982, in Comets, ed. L. L. Wilkening (Tucson: Univ. Arizona Press), 131
Greenberg, J. M., & Li, A. 1996, A&A, 309, 258
Greenberg, J. M., Li, A., Mendoza-Gómez, C. X., Schutte, W. A., Gerakines, P. A., & de Groot, M. 1995, ApJ, 455, L177
Grishko, V. I., & Duley, W. W. 2002, ApJ, 568, 448
Günzler, H., & Heise, H. M. 1996, IR-Spektroskopie (3rd ed.; Weinheim: Wiley-VCH)
Haaland, P. D., Garscadden, A., Ganguly, B., Ibrani, S., & Williams, J. 1994, Plasma Sources Sci. Technol., 3, 381
Imanishi, M. 2000a, MNRAS, 313, 165
———. 2000b, MNRAS, 319, 331
———. 2002, ApJ, 569, 44
Imanishi, M., & Dudley, C. C. 2000, ApJ, 545, 701
Imanishi, M., Dudley, C. C., & Maloney, P. R. 2001, ApJ, 558, L93
Imanishi, M., & Maloney, P. R. 2003, ApJ, 588, 165
Imanishi, M., Terada, H., Sugiyama, K., Motohara, K., Goto, M., & Maihara, T. 1997, PASJ, 49, 69
Jura, M. 1990, ApJ, 365, 317
Kobayashi, H., Bell, A. T., & Shen, M. 1974, Macromolecules, 7, 277
Kovačević, E., Stefanović, I., Berndt, J., & Winter, J. 2003, J. Appl. Phys., 93, 2924

Lacy, J. H., Baas, F., Allamandola, L. J., Persson, S. E., McGregor, P. J., Lonsdale, C. J., Geballe, T. R., & van de Bult, C. E. P. 1984, ApJ, 276, 533
Marco, O., & Brooks, K. J. 2003, A&A, 398, 101
Mason, R. E., Wright, G., Pendleton, Y., & Adamson, A. 2004, ApJ, 613, 770
Mennella, V., Brucato, J. R., Colangeli, L., & Palumbo, P. 1999, ApJ, 524, L71
Mennella, V., Palumbo, M. E., & Baratta, G. A. 2004, ApJ, 615, 1073
Meyer, D. M., Cardelli, J. A., & Sofia, U. J. 1997, ApJ, 490, L103
Mizutani, K., Suto, H., & Maihara, T. 1994, ApJ, 421, 475
Neckel, T., & Staude, H. J. 1987, ApJ, 320, L145
Palumbo, M. E., Pendleton, Y. J., & Strazzulla, G. 2000, ApJ, 542, 890
Pendleton, Y. J. 1997a, in The Cosmic Dust Connection, ed. J. M. Greenberg (NATO ASI Ser. C, 487) (Dordrecht: Kluwer), 71
———. 1997b, Origins Life Evol. Bios., 27, 53
———. 2004, in ASP Conf. Ser. 309, Astrophysics of Dust, ed. A. N. Witt, G. C. Clayton, & B. T. Draine (San Francisco: ASP), 573
Pendleton, Y. J., & Allamandola, L. J. 2002, ApJS, 138, 75
Pendleton, Y. J., Sandford, S. A., Allamandola, L. J., Tielens, A. G. G. M., & Sellgren, K. 1994, ApJ, 437, 683
Pendleton, Y. J., Tielens, A. G. G. M., Tokunaga, A. T., & Bernstein, M. P. 1999, ApJ, 513, 294
Perrin, J., & Hollenstein, C. 1999, in Dusty Plasmas, ed. A. Bouchoule (New York: Wiley), 77
Praburam, G., & Goree, J. 1995, ApJ, 441, 830
Rawlings, M. G., Adamson, A. J., & Whittet, D. C. B. 2003, MNRAS, 341, 1121
Risaliti, G., et al. 2003, ApJ, 595, L17
Robertson, J. 1991, in Diamond and Diamond-like Films and Coatings, ed. R. E. Clausing, L. L. Horton, J. C. Angus, & P. Koidl (NATO ASI Ser. B, 266) (New York: Plenum), 331
Sandford, S. A., Allamandola, L. J., Tielens, A. G. G. M., Sellgren, K., Tapia, M., & Pendleton, Y. 1991, ApJ, 371, 607
Sandford, S. A., Pendleton, Y. J., & Allamandola, L. J. 1995, ApJ, 440, 697
Schnaiter, M., Mutschke, H., Dorschner, J., Henning, T., & Salama, F. 1998, ApJ, 498, 486
Schutte, W. A., Greenberg, J. M., van Dishoeck, E. F., Tielens, A. G. G. M., Boogert, A. C. A., & Whittet, D. C. B. 1997, Ap&SS, 255, 61
Socrates, G. 1980, Infrared Characteristic Group Frequencies (New York: Wiley)
Soifer, B. T., Russell, R. W., & Merrill, K. M. 1976, ApJ, 207, L83
Spoon, H. W. W., Moorwood, A. F. M., Pontoppidan, K. M., Cami, J., Kregel, M., Lutz, D., & Tielens, A. G. G. M. 2003, A&A, 402, 499
Stefanović, I., Kovačević, E., Berndt, J., & Winter, J. 2003, New J. Phys., 5, 39
Stoykov, S., Eggs, C., & Kortshagen, U. 2001, J. Phys. D, 34, 2160
Swinkels, G. H. P. M., Kersten, H., Deutsch, H., & Kroesen, G. M. W. 2000, J. Appl. Phys., 88, 1747
Whittet, D. C. B., Pendleton, Y. J., Gibb, E. L., Boogert, A. C. A., Chiar, J. E., & Nummelin, A. 2001, ApJ, 550, 793
Whittet, D. C. B., et al. 1997, ApJ, 490, 729
Woolf, N. J., & Ney, E. P. 1969, ApJ, 155, L181
Wright, G. S., Bridger, A., Geballe, T. R., & Pendleton, Y. 1996, in New Extragalactic Perspectives in the New South Africa, ed. D. L. Block & J. M. Greenberg (Dordrecht: Kluwer), 143